NASA/TM—2009-216088 AIAA–2009–4012

Numerical Studies of a Fluidic Diverter for Flow Control

Suleyman A. Gokoglu, Maria A. Kuczmarski, and Dennis E. Culley
Glenn Research Center, Cleveland, Ohio

Surya Raghu
Advanced Fluidics LLC, Columbia, Maryland

December 2009

NASA STI Program . . . in Profile

Since its founding, NASA has been dedicated to the advancement of aeronautics and space science. The NASA Scientific and Technical Information (STI) program plays a key part in helping NASA maintain this important role.

The NASA STI Program operates under the auspices of the Agency Chief Information Officer. It collects, organizes, provides for archiving, and disseminates NASA's STI. The NASA STI program provides access to the NASA Aeronautics and Space Database and its public interface, the NASA Technical Reports Server, thus providing one of the largest collections of aeronautical and space science STI in the world. Results are published in both non-NASA channels and by NASA in the NASA STI Report Series, which includes the following report types:

- TECHNICAL PUBLICATION. Reports of completed research or a major significant phase of research that present the results of NASA programs and include extensive data or theoretical analysis. Includes compilations of significant scientific and technical data and information deemed to be of continuing reference value. NASA counterpart of peer-reviewed formal professional papers but has less stringent limitations on manuscript length and extent of graphic presentations.

- TECHNICAL MEMORANDUM. Scientific and technical findings that are preliminary or of specialized interest, e.g., quick release reports, working papers, and bibliographies that contain minimal annotation. Does not contain extensive analysis.

- CONTRACTOR REPORT. Scientific and technical findings by NASA-sponsored contractors and grantees.

- CONFERENCE PUBLICATION. Collected papers from scientific and technical conferences, symposia, seminars, or other meetings sponsored or cosponsored by NASA.

- SPECIAL PUBLICATION. Scientific, technical, or historical information from NASA programs, projects, and missions, often concerned with subjects having substantial public interest.

- TECHNICAL TRANSLATION. English-language translations of foreign scientific and technical material pertinent to NASA's mission.

Specialized services also include creating custom thesauri, building customized databases, organizing and publishing research results.

For more information about the NASA STI program, see the following:

- Access the NASA STI program home page at *http://www.sti.nasa.gov*

- E-mail your question via the Internet to *help@sti.nasa.gov*

- Fax your question to the NASA STI Help Desk at 443–757–5803

- Telephone the NASA STI Help Desk at 443–757–5802

- Write to:
  NASA Center for AeroSpace Information (CASI)
  7115 Standard Drive
  Hanover, MD 21076–1320

NASA/TM—2009-216088 AIAA–2009–4012

Numerical Studies of a Fluidic Diverter for Flow Control

Suleyman A. Gokoglu, Maria A. Kuczmarski, and Dennis E. Culley
Glenn Research Center, Cleveland, Ohio

Surya Raghu
Advanced Fluidics LLC, Columbia, Maryland

Prepared for the
39th Fluid Dynamics Conference and Exhibit
sponsored by the American Institute of Aeronautics and Astronautics
San Antonio, Texas, June 22–25, 2009

National Aeronautics and
Space Administration

Glenn Research Center
Cleveland, Ohio 44135

December 2009

Acknowledgments

The authors gratefully acknowledge the support of this work by the NASA Fundamental Aeronautics program, Subsonic Fixed Wing project.

This work was sponsored by the Fundamental Aeronautics Program at the NASA Glenn Research Center.

Level of Review: This material has been technically reviewed by technical management.

Available from

NASA Center for Aerospace Information
7115 Standard Drive
Hanover, MD 21076–1320

National Technical Information Service
5285 Port Royal Road
Springfield, VA 22161

Available electronically at http://gltrs.grc.nasa.gov

Numerical Studies of a Fluidic Diverter for Flow Control

Suleyman A. Gokoglu, Maria A. Kuczmarski, and Dennis E. Culley
National Aeronautics and Space Administration
Glenn Research Center
Cleveland, Ohio 44135

Surya Raghu
Advanced Fluidics LLC
Columbia, Maryland 21045

The internal flow structure in a specific fluidic diverter is studied over a range from low subsonic to sonic inlet conditions by a time-dependent numerical analysis. The understanding will aid in the development of fluidic diverters with minimum pressure losses and advanced designs of flow control actuators. The velocity, temperature and pressure fields are calculated for subsonic conditions and the self-induced oscillatory behavior of the flow is successfully predicted. The results of our numerical studies have excellent agreement with our experimental measurements of oscillation frequencies. The acoustic speed in the gaseous medium is determined to be a key factor for up to sonic conditions in governing the mechanism of initiating the oscillations as well as determining its frequency. The feasibility of employing plasma actuation with a minimal perturbation level is demonstrated in steady-state calculations to also produce oscillation frequencies of our own choosing instead of being dependent on the fixed-geometry fluidic device.

1.0 Introduction

Almost any aerodynamic problem can be mitigated in the laboratory through the proper application of flow control techniques (Ref. 1). In each flow control application, the common denominator is that it requires some type of actuation mechanism. The specific implementation can be passive or active, open-loop or closed-loop; however, with every benefit there is a corresponding penalty when evaluated at the system level. In any practical application, the determining factor in whether to implement flow control at all is in the net effect to the system. Due to this inescapable fact, the actuation mechanism and its ancillary support structure are the determining elements in understanding the penalty aspect of flow control. Nowhere is this more apparent than in internal flow control applications in turbomachinery (Refs. 2 and 3).

The ideal actuator for maximizing flow control benefit must develop sufficient control authority (e.g., velocity, momentum, frequency, etc.) at a location which requires the minimum control authority (i.e., where it is most effective). The efficiency of the actuator is a function of the magnitude of the energy transferred to the problematic flow and its spatial extent and direction. The objective is typically not to alter the freestream flow directly because of the excessive energy requirement, but to leverage, or redistribute, the freestream energy to achieve the desired effect. In actuality, the size of the actuation device always matters, and its ability to focus energy in a much localized space is perhaps the most important characteristic.

The simplest flow control (or flow management) devices are passive vortex generators, such as ramps or miniature vanes with no moving parts. The simplicity of these devices makes them desirable for some applications because they are effective and robust and extend aerodynamic performance in off-design situations. While they require no external power to operate, they reduce aerodynamic performance when not needed.

Active flow control devices (whether open or closed-loop) try to minimize the performance penalty by only being activated, and therefore, affecting the flow during off-design operations. While active devices have the potential for maximizing operational benefits, the total impact is often negated by the

added complexity, weight, power, cost, and unreliability to the system. Flow control actuators that approximate the ideal are active devices that minimize these system costs.

In turbomachinery, potential applications exist in every component of the engine, some of which can be listed as follows: (1) Inlet—separation control, boundary layer control, distortion control; (2) Fan—noise (wake) reduction; (3) Compressor—stator separation control, stability control, stage matching; (4) Combustor—mixing; (5) Turbine—cooling control, cooling efficiency, stator separation control, transition duct separation control; and (6) Nozzle—jet noise reduction.

Fluidic diverters, as described in this paper and in Reference 4, are actively controlled actuators which inject fluid into the freestream in an unsteady, periodic manner. While the devices require a source of pressurized fluid, they have no moving parts, add little to no weight, and require no external power for operation. Furthermore, the devices can be scaled over a great extent in terms of size, periodic frequency, and flow rate.

2.0 The Fluidic Diverter

A schematic of a generic fluidic diverter is shown in Figure 1. The jet created at the end of the converging section is bi-stable in nature and steers to one side of the wall attachment region provided in the chamber due to the Coanda effect (Refs. 5 and 6), the tendency of a fluid jet to stay attached to an adjacent curved surface. A part of the momentum or the pressure pulse is transmitted back through the feedback channel, which switches the jet attachment from one side to the other side of the chamber. Thus, the jet of fluid is diverted alternately into the two outlets provided at the exit.

The frequency characteristics of the fluidic diverter greatly depend on the design of the internal geometry of the wall attachment region and the feedback channels. Fluidic oscillators typically have linear flow versus frequency characteristics until sonic conditions are achieved at the converging section, and then show saturation beyond this flow rate. Pulse frequencies from 1 to 10 kHz have been obtained with meso-scale (nozzle sizes in the range of 200 μm to 1 mm) fluidic actuators with very low mass flow rates of the order of (0.05 to 0.5 gm/s).

An example of the concept of flow control using such an array of fluidic diverters in a stator vane is shown in Figure 2. Pulsing jets with sufficient authority (velocity amplitude ratio $u/U \sim 1$) slightly ahead of the separation line leverages the high momentum freestream flow to cause reattachment of the separated flow on the suction-side surface. The reattachment will minimize the wake downstream of the stator vane under off-design conditions and reduce losses. This enables higher vane loading which can result in lower solidity, that is, fewer vanes per stage, or even a reduced number of stages to achieve the same pressure rise in the compressor.

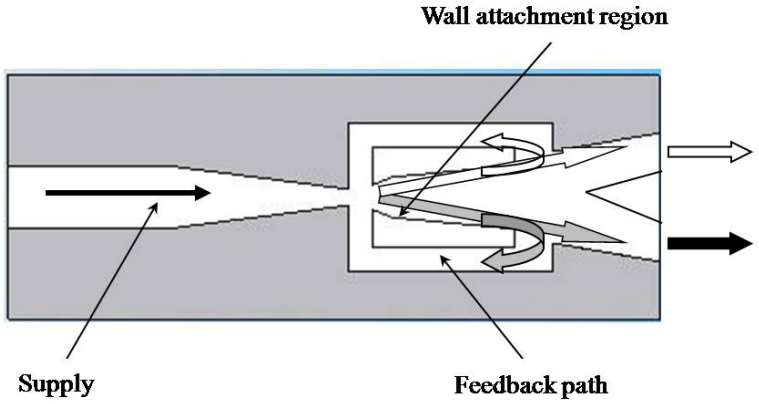

Figure 1.—Schematic of a fluidic diverter.

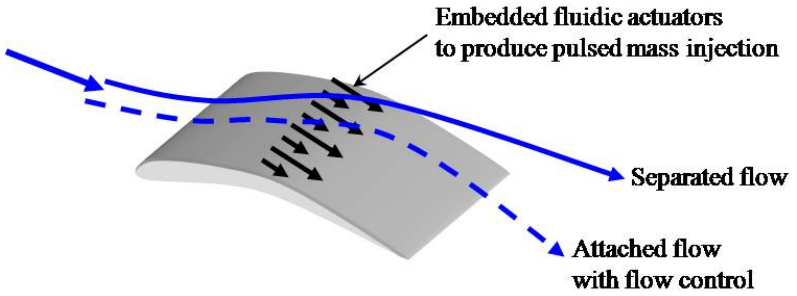

Figure 2.—Separation control using pulsed mass-flow injection with fluidic diverter arrays.

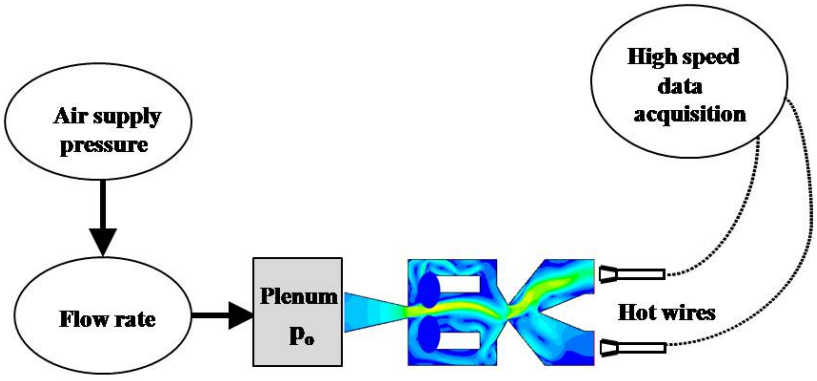

Figure 3.—A simple schematic of the experimental setup.

3.0 Motivation and Objectives

The motivation for this study comes from the desire to develop robust actuators that can function over a range from low subsonic to sonic inlet conditions. The specific objective of this paper is to understand the internal flow structure and the physics of the oscillation mechanisms in such a fluidic diverter by a time-dependent numerical analysis. This understanding will aid in the development of fluidic diverters with minimum pressure losses and advanced designs of flow control actuators. The velocity, temperature and pressure fields are calculated for subsonic conditions and the self-induced oscillatory behavior of the flow is successfully predicted. The results of our numerical studies compared remarkably well to our experimental measurements of oscillation frequencies.

4.0 Experimental Measurements

Accompanying experiments are performed to support the numerical modeling effort and to better understand the switching dynamics of the fluidic diverter. A more detailed description of the experimental setup and measurement techniques are given in Reference 7. A simpler schematic is shown in Figure 3 below. Hot wires are positioned at the approximate center of the device's two outlets to monitor the state of the air flow through the diverter and to determine the frequency of oscillations of the flow between the two outlets. The reported frequencies are stated with respect to each outlet, that is, each outlet produces a pulsation of identical frequency but opposite phase.

The flow at each outlet is similar in some respects to a synthetic jet because there is a period of outflow followed by a small amount of inflow. Obviously the ratio of outflow to inflow is highly skewed since the device requires a pressure source.

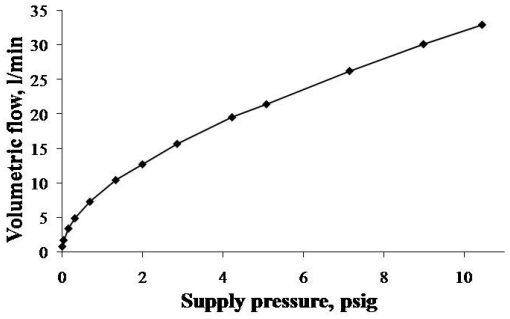

Figure 4.—The measured relationship between the air supply pressure and the volumetric flow rate through the fluidic diverter.

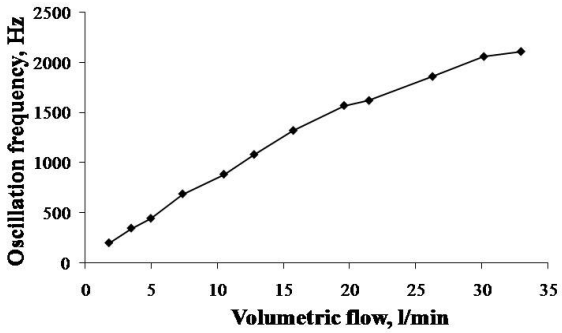

Figure 5.—The measured relationship between the volumetric flow rate through the fluidic diverter and the oscillation frequency.

The air supply pressure and the corresponding flow rate (Fig. 4) and outlet oscillation frequencies (Fig. 5) are recorded via a high-speed data acquisition system. The measured air supply pressure is obtained very near to the plenum, within 3 in., and is assumed to have negligible pressure drop before entering the device inlet.

The agreement between the numerically predicted and measured oscillations is excellent and described below.

5.0 Discussion of Numerical Results

The numerical investigation uses the standard commercial CFD software FLUENT 6. The computational domain is two-dimensional (2–D). It uses the beginning of the converging nozzle originating from the supply plenum at constant pressure and 298 K as the inlet boundary condition and opens to the ambient environment at 1 atm and 298 K at the two outlets. The numerical mesh is built with standard rules and the sensitivity of the calculations with respect to the grid size is checked to ascertain sufficient resolution. As a result, the calculations use a mixture of structured and unstructured 134,106 quadrilateral mesh elements (266,349 interior faces, 3,406 wall faces, 204 2–D pressure outlet faces, and 116 2–D pressure inlet faces). Grid adaption is not deemed necessary for the subsonic cases of current focus, and the calculations are done for compressible turbulent flow. The total pressure at the inlet (in the supply plenum) is specified. The walls are assumed to be at constant ambient temperature of 298 K.

The analysis is done nominally for five different supply plenum pressures that correspond approximately to a Mach-number range from 0.1 to 0.9. For smaller Mach numbers, the corresponding Reynolds number is also smaller, and hence, requires the effects transition from laminar to fully turbulent flow to be considered. Assuming isentropic conditions, the correspondence between the supply plenum pressure and the Mach number is given in Table I.

TABLE I.—SUPPLY PLENUM PRESSURE AND MACH NUMBER ANALYSIS

Mach no.	p_o, atm
0.1	1.007
0.3	1.064
0.5	1.186
0.8	1.480
0.9	1.691

5.1 Steady-State Calculations

The approach is to tune the numerical parameters of the model with steady-state calculations, determine the most appropriate turbulence model for our conditions, and make sure that the results are completely consistent before undertaking any time-dependent calculations. Naturally, these steady-state cases do not capture the oscillatory behavior of the diverter, but they give invaluable hints as to the proper application of various turbulence models and the accuracy of results.

We have applied three different turbulence models: (1) *k*-ε turbulence model with standard wall functions, (2) *k*-ε turbulence model with enhanced wall functions, and (3) *k*-ω turbulence model with shear stress transport (SST). For all three turbulence models, the numerical mesh is structured such that it is neither too fine for the wall function approach nor too coarse for the enhanced wall treatment approach. Since the low Mach number cases are also relatively low Reynolds number cases for our conditions, we enable the transitional flow option in FLUENT. Therefore, the *k*-ω model employs the same guidelines as the enhanced wall treatment.

A portion of the fluidic diverter modeled in this study is camouflaged in the figures presented below due the commercially sensitive nature of the information, but the physics of the phenomena can easily be followed without any sacrifice.

5.1.1 *k*-ε Turbulence Model With Standard Wall Functions

First, we have employed the *k*-ε turbulence model with standard wall functions which work reasonably well for the treatment of near-wall regions when the constant-shear and local equilibrium hypotheses are valid; that is, no severe pressure gradients. The grid is structured such that it is neither too small near the wall nor too coarse in the fully turbulent region. The results for velocity magnitude, temperature and pressure fields of a typical Ma = 0.3 case are shown in Figure 6.

The solution converges smoothly and the flow looks quite symmetric. Given the bi-stable nature of the flow for this diverter, the fact that the flow remains so symmetric indicates that the level of numerical accuracy is sufficiently high and does not generate a large enough perturbation to break the flow symmetry. The Coanda effects are observed in the central chamber where the flow attaches itself to the side walls. Since the Mach number is not large, the effect of high-speed cooling is minimal. The pressure drops in the initial converging nozzle section from its initial plenum level and remains relatively uniform in the mid-section and exit region.

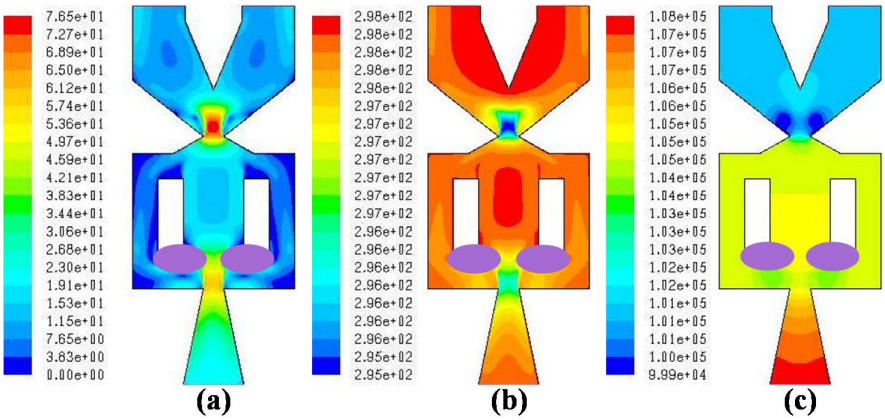

Figure 6.—Ma = 0.3, the *k*-ε turbulence model with standard wall functions, (a) velocity magnitude (m/s), (b) temperature (K), and (c) pressure (pascal).

5.1.2 *k*-ε Turbulence Model With Enhanced Wall Functions

Next, we have tried the *k*-ε turbulence model with enhanced wall functions. This method treats the entire near-wall region (i.e., laminar sublayer, buffer region, and fully-turbulent outer region) with a single formulation by blending linear (laminar) and logarithmic (turbulent) laws-of-the-wall. The results for the velocity magnitude fields are shown side by side in Figure 7 for the original standard wall functions and enhanced wall functions cases. Although there are differences in the predictions, the general trends and the symmetry of the flow fields are preserved in both cases.

5.1.3 *k*-ω Turbulence Model With Shear Stress Transport

It is known for compressible turbulent flows that the *k*-ω turbulence model with shear stress transport (SST) offers a more accurate treatment of the near-wall region and is reliable for a wider class of flows, including cases with adverse pressure gradients (as is the situation with the Coanda effect). Therefore, we have next focused on this model. This approach also gives flow fields with symmetry, but seems to have more jet-flow behavior, as shown in Figure 8. The accuracy of the predictions is checked by a systematic

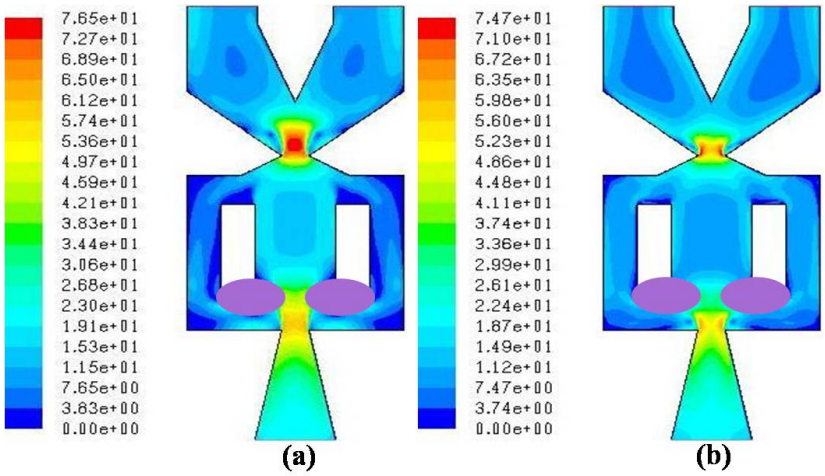

Figure 7.—Ma = 0.3, velocity magnitude fields (m/s) using the *k*-ε turbulence model with (a) standard wall functions and (b) enhanced wall functions.

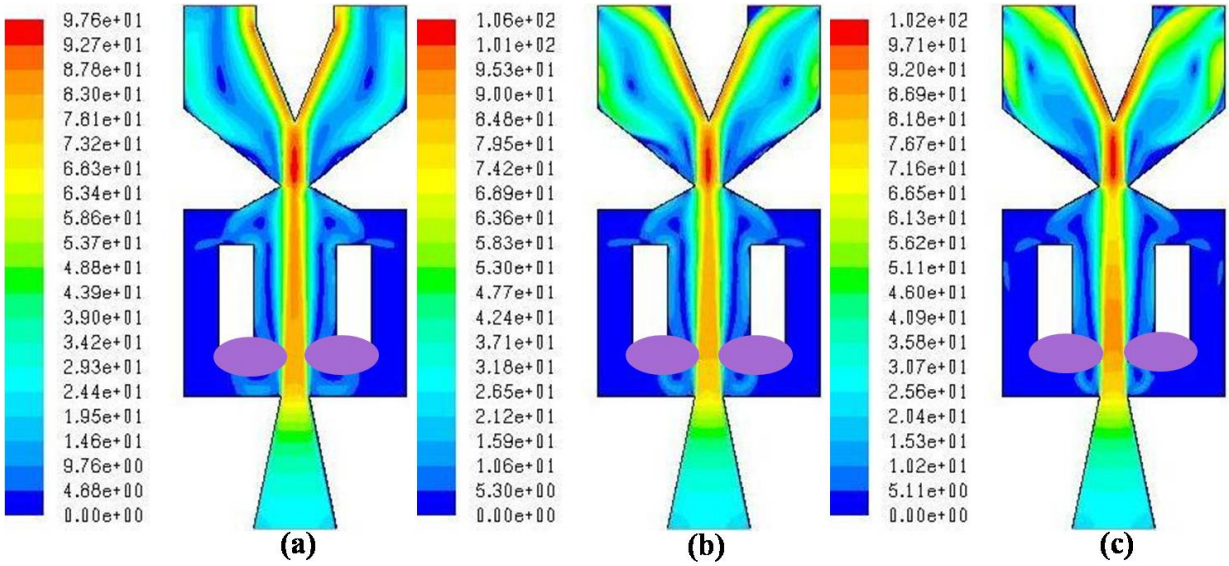

Figure 8.—Ma = 0.3, velocity magnitude fields (m/s) using the *k*-ω turbulence model with SST for grid densities of (a) *n* = 10, (b) *n* = 20, and (c) *n* = 30.

study of various numerical parameters and schemes. Figure 8 shows the results obtained by varying the grid density, which is accomplished by varying the number of cells (n = 10, 20, or 30) put across the smallest segment in the domain as the numerical grid is generated. In general, grid densities affect convergence and flow symmetry, and deterioration in numerical accuracy leads to convergence problems depending on the flow rate (Mach number). For the Ma = 0.3 case depicted in Figure 8, all three grid densities tried seem to be reasonably close to one another. However, for the whole Mach number range between 0.1 to 0.9, we reach the conclusion that this diverter can be most accurately modeled by using the k-ω turbulence model with SST and incorporating effects of transitional flow, grid density of n = 20, and 2nd-order upwind solution scheme.

Before we embark on time-dependent calculations, we have also tested the feasibility of using active means of actuating the oscillation mechanism. Of interest is using an electrically induced plasma disturbance (Refs. 8 and 9) in place of the passive feedback channels used in the typical device. The concept is to employ a controlled disturbance, capable of frequencies commensurate with the fluidic device capabilities, to produce a high authority output over a broad range of frequencies of our own choosing instead of being dependent on the fixed geometry. The objective here is to quantify the minimum level of perturbation necessary to break the steady-state flow symmetry or switch the flow direction when the steady-state flow is already biased in one direction. The plasma actuation is simulated by applying a numerically-patched "plasma" to a local area of given height and width in the nozzle exit region as shown in Figure 9. In this local area, the temperature of the "live" cells (which otherwise participate in the flow calculations) is set to a prescribed value after a pre-existing steady flow field is established. First, the patch is applied on the left-hand side over an initially symmetric flow field. Calculations are run to establish a new steady flow field. Then, the left-side patch is eliminated and a new patch is applied on the opposite right-hand side over the newly generated flow field in order to simulate the successive switching of the flow direction at the outlet.

Indeed, for the range of flow rates we have tried in this paper, a "plasma" temperature as low as 1300 K is sufficient (a) to break the original steady-state flow symmetry when applied from one side in the nozzle exit region, and (b) to switch the flow direction to the opposite outlet when the flow was originally biased to one outlet. The results are shown in Figure 10 for the Ma = 0.3 case.

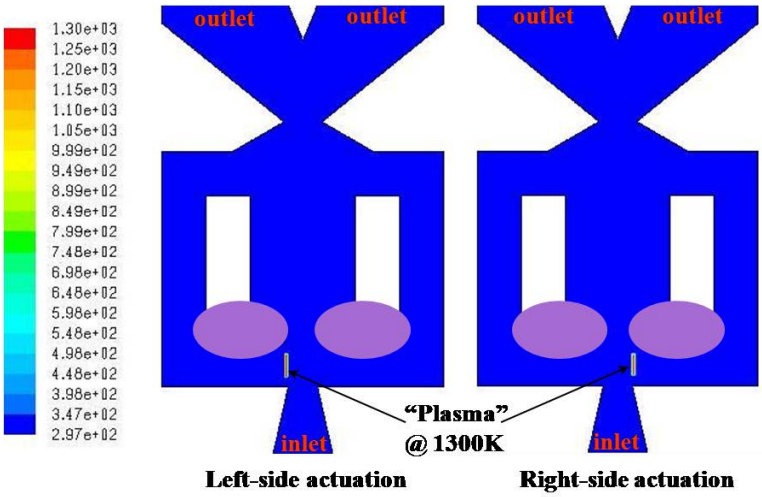

Figure 9.—"Plasma" actuation by a high-temperature numerical patch.

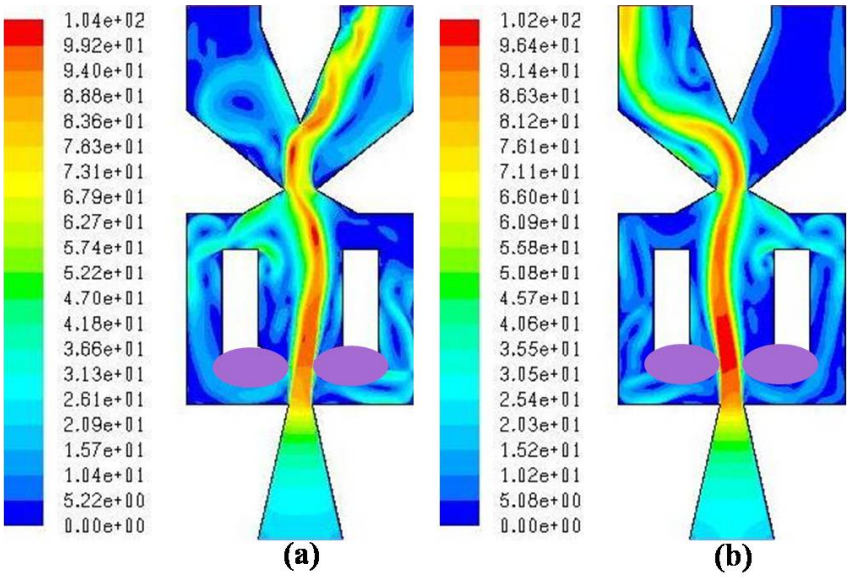

Figure 10.—Ma = 0.3, velocity magnitude fields (m/s) for "plasma" at 1300 K, (a) left-side actuation of originally symmetric flow, (b) right-side actuation after left-side actuation as in (a).

5.2 Time-Dependent Calculations

With the numerical parameters determined in steady-state calculations and with the confidence developed for the accuracy of the computations, we have shifted our focus to time-dependent calculations. We have been able to generate self-induced oscillations for all subsonic cases we have tried. A constant time step of 10^{-5} sec is found to be sufficiently accurate for all Mach numbers. Initially, the pressure-based segregated (uncoupled) algorithm was utilized for relatively small Mach numbers, but subsequently, a pressure-based coupled solver is adopted as the more robust approach (Ref. 10).

Four sets of time-series calculations are presented below, two sets for the typical case of Ma = 0.3 shown in Figures 11 and 12, and the other two sets for the highest Mach number case of 0.9 shown in Figures 14 and 15.

For Ma = 0.3, the first time-series graphs shown in Figure 11 demonstrate the symmetric initiation of the flow until the onset of the first oscillation. The initial flow continues with a symmetric structure for the first 1.3 ms, but loses its stability in about 2.2 ms to direct itself to the outlet on the right. It then switches to the left outlet by 2.7 ms.

The second time-series graphs for Ma = 0.3, shown in Figure 12 between 9.0 and 10.5 ms, demonstrate the typical oscillations, that develop after a brief initial delay (approx. 2.2 ms), along with their associated profiles of the vertical component of the exit velocity perpendicular to the exit plane for each outlet. The rows of figures show that the oscillation pattern is regular with a uniform periodicity. In fact, for all Mach numbers studied in this paper, calculations carried out for longer times confirm that the oscillation frequencies remain steady. The predicted oscillation frequency for this case is 760 Hz and is in excellent agreement with the experimental measurements, as reported below.

The color plots of the velocity magnitude in Figure 12 at 9.0 and 9.3 ms indicate that the oscillating flow is moving toward the left edge of the left outlet during this period. The velocity profile at 9.0 ms shows that there is suction into the right outlet with flow recirculation rolls developing inside. By 9.3 ms, the flow in the left outlet moves more to the left while the right exit region stagnates. At 9.6 ms, almost a mirror image of the flow structure seen at 9.0 ms is developed. Similarly, the flow structure at 9.9 ms is almost a mirror image of that at 9.3 ms. The color plots at 10.2 and 10.5 ms show that the cycle is

completed, with respective flow structures looking very similar to those at 9.0 and 9.3 ms. Note that the maximum velocity of 112 m/s (Ma ≈ 0.3) is reached when the flow is in the central wall-attachment section of the diverter, between the top nozzle (the neck opening to the outlet channels) and the bottom nozzle.

For the Ma = 0.3 case, the maximum value of the vertical component of the exit velocity for the snapshots series shown is around 70 m/s (see Fig. 12 at 9.0 ms), corresponding to a local Mach number of about 0.2.

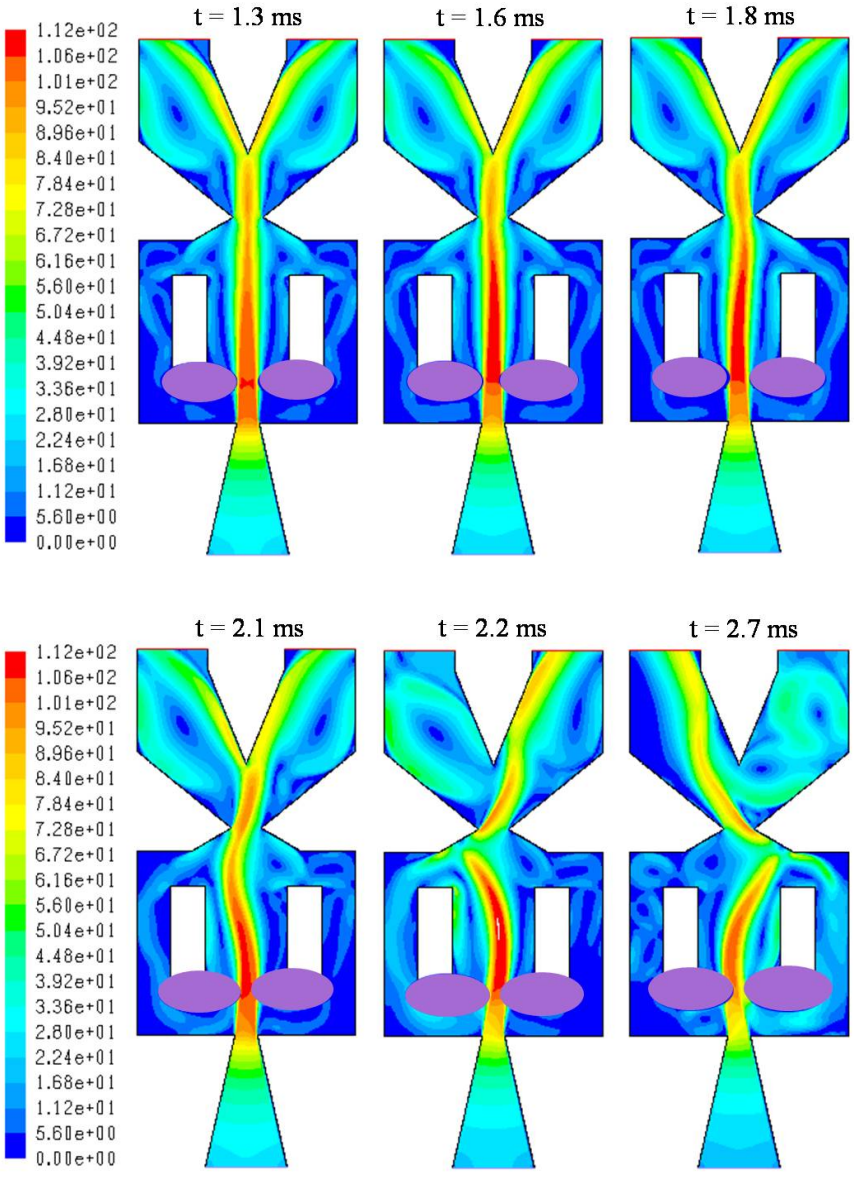

Figure 11.—Ma = 0.3, velocity magnitude fields (m/s), snapshots taken at indicated times (ms) showing the initiation of oscillations.

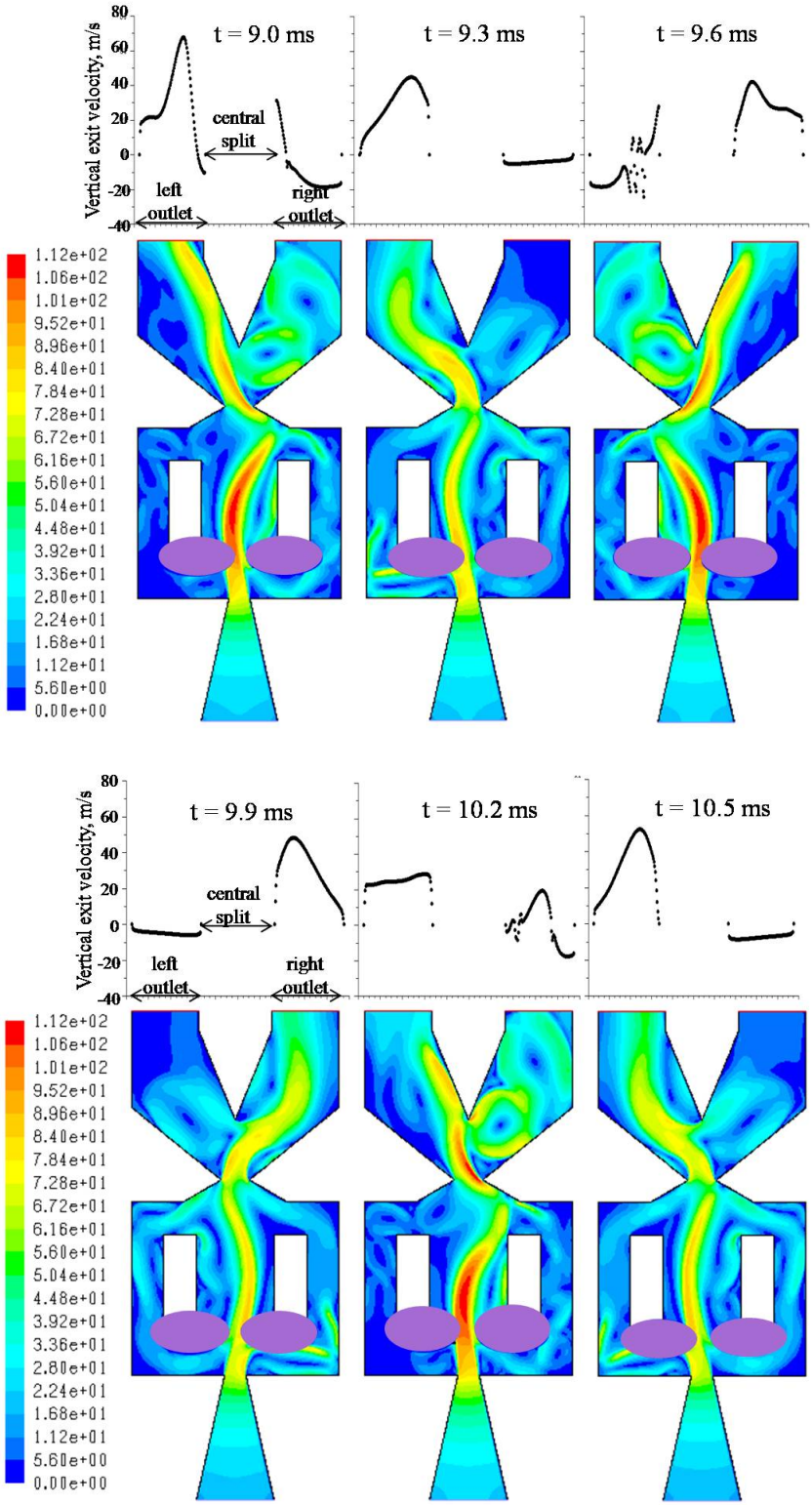

Figure 12.—Ma = 0.3, velocity magnitude fields (m/s), snapshots taken at indicated times (ms) showing regular oscillations (below) and their associated profiles of vertical exit velocity for each outlet (above).

Flow direction and profile at the exit planes as well as inside the outlet channels are more clearly demonstrated by velocity vector plots. Figure 13 shows the velocity vectors in the outlet channels of the Ma = 0.3 case and depicts the suction from outside, recirculation directions, and stagnation zones of the flow at 9.0, 9.3, and 9.6 ms, spanning a duration of approximately one-half cycle of oscillation. The velocity vector magnitudes are scaled and colored at prescribed grid locations in order to enhance visual clarity. The exit velocity profiles shown in Figure 12 are for the vertical component of the vector profiles shown in Figure 13.

For Ma = 0.9, similar sets of graphs as for Ma = 0.3 are generated. Graphs shown in Figure 14 demonstrate again the symmetric initiation of the flow until 0.5 ms, after which it gradually loses its symmetry, and eventually leads to the outlet on the right by about 0.8 ms, and switches to the left outlet by 1.0 ms. Note that the first onset of instability leading to oscillations occurs faster for this higher flow rate (0.8 ms for Ma = 0.9 versus 2.2 ms for Ma = 0.3).

The second time-series graphs for Ma = 0.9, shown in Figure 15 between 9.5 and 10.0 ms, also demonstrate the typical oscillations that develop as in Figure 12, except the oscillation frequency is now about 2250 Hz. In fact, the oscillation frequency increases linearly with Mach number (i.e., source pressure or flow rate), which is in excellent agreement with the frequencies measured experimentally, as shown in Figure 17.

The color plots of the velocity magnitude in Figure 15 between 9.5 and 9.7 ms indicate that the oscillating flow is moving from the right outlet to the left outlet during this period. The velocity profile at 9.9 ms shows that there is significant amount of suction into the left outlet reaching downward velocities greater than 100 m/s at the exit plane. Relatively stagnant conditions are observed at 9.6 ms on the left and at 9.8 ms on the right outlet closer to exits with a flow recirculation roll generated inside both. The flow structures are regularly repeated for each cycle and reflected symmetrically between the left and right outlets.

For this Ma = 0.9 case, the maximum value of the vertical component of the exit velocity during the series of snapshots shown is approximately 250 m/s (see Fig. 15 at 9.9 ms), corresponding to a local Mach number of little over 0.7. Note also that the velocity of the flow emerging from the top nozzle towards the outlet channels can be larger than the one which develops in the central wall-attachment section. This is because the flow is not steady and is not unidirectional going through successive nozzles. The unsteady nature of the flow changes the “effective” area of (especially) the second (top) nozzle and the angle at which the flow enters, passes, and emerges from the second nozzle in an oscillatory manner. During these periodic variations, at certain snapshots, the flow can accelerate through smaller effective cross-sectional areas and the velocities do become locally larger than those emerging from the first (bottom) nozzle into the central wall-attachment section. The vertical pulsations (axial pumping action) renders the emerging flow even from the first nozzle unsteady, periodically changing its velocity magnitude (and direction) with time.

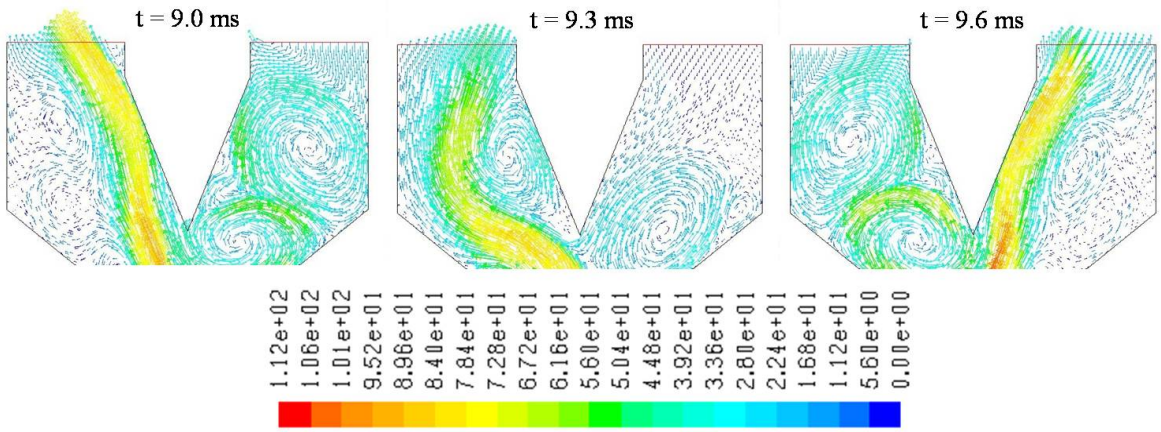

Figure 13.—Ma = 0.3, velocity vectors (m/s, scale shown sideways) snapshots taken at indicated times (ms) showing flow direction (suction) at exit planes, recirculation rolls, and stagnation zones in outlet channels.

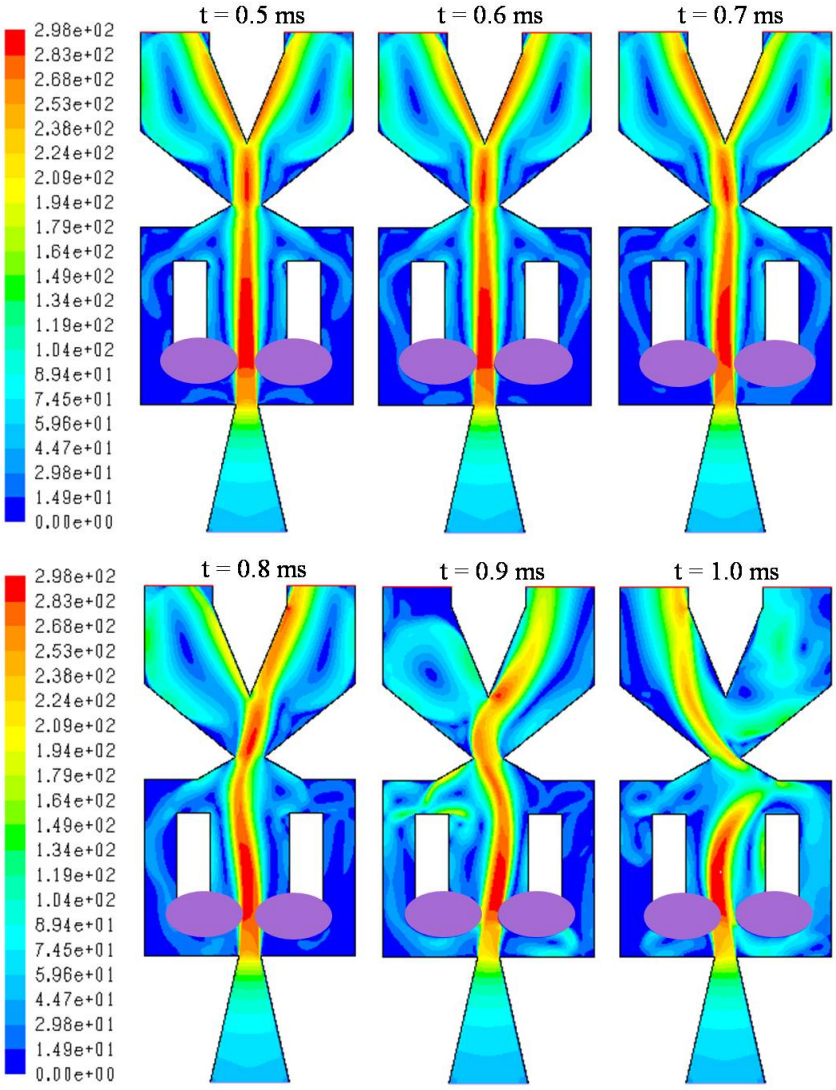

Figure 14.—Ma = 0.9, velocity magnitude fields (m/s), snapshots taken at indicated times (ms) showing the initiation of oscillations.

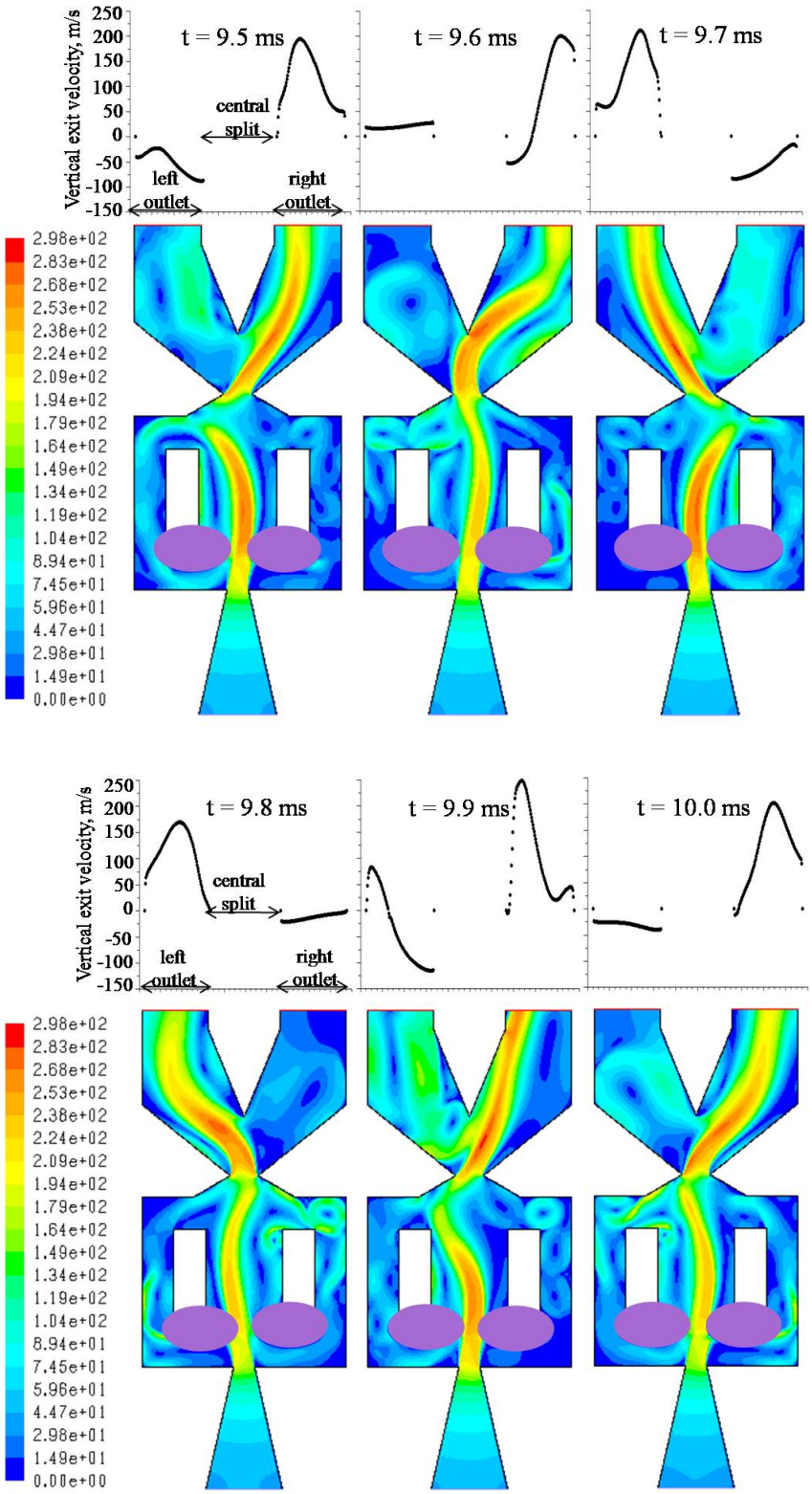

Figure 15.—Ma = 0.9, velocity magnitude fields (m/s), snapshots taken at indicated times (ms) showing regular oscillations (below) and their associated profiles of vertical exit velocity for each outlet (above).

Figure 16 shows the velocity vectors in the outlet channels of the Ma = 0.9 case. The snapshots taken at 9.8, 9.9, and 10.0 ms depict the direction of the flow as well as the recirculation rolls over a period of approximately one-half cycle of oscillation. It can be seen that the significant level of suction generated at 9.9 ms on the left side produces velocities on the order of 200 m/s inside the outlet, while the on the left the exit velocities exceed 260 m/s. The exit velocity profiles shown in Figure 15 are for the vertical component of the vector profiles shown in Figure 16.

Note that the angle of departure of the flow (relative to the exit plane) leaving the outlets keeps varying during the oscillations, as shown in both Figures 13 and 16 for Ma = 0.3 and 0.9, respectively. These sideway sweeping motions (as well as the vertical pulsations as mentioned above) can be helpful in increasing the effectiveness of the fluidic diverter by providing more efficient penetration into and/or mixing with the freestream flowing over the outlets.

As an aside, the authors conjecture that this sweeping motion can be used in film cooling applications to increase film cooling efficiency. Of course, the film cooling application is attempting to minimize any disturbance to the flow field, which is completely opposite of most flow control applications.

Because the calculations here are 2–D, we limit our discussions mainly to the effects of the exit velocities from the fluidic diverter outlets. Two-dimensional calculations do not allow us to evaluate the effects of momentum exchange between the diverter flow and the mainstream since these effects would also require knowing such factors as the area, shape, and the geometric angle of the outlet exit relative to the outside surface.

The frequencies of oscillations generated by the fluidic diverter are measured experimentally by using room temperature air as described briefly in Section 4.0. The stated frequency is with respect to each outlet. Figure 17 shows that the measured and numerically calculated frequencies as a function of the Mach number. The Mach number is calculated by assuming isentropic flow and by using either the measured air supply pressure or the plenum pressure applied as a numerical inlet boundary condition. The agreement between the experimentally measured and numerically calculated oscillation frequencies is excellent for the full of range of Mach numbers from 0.1 to 0.9.

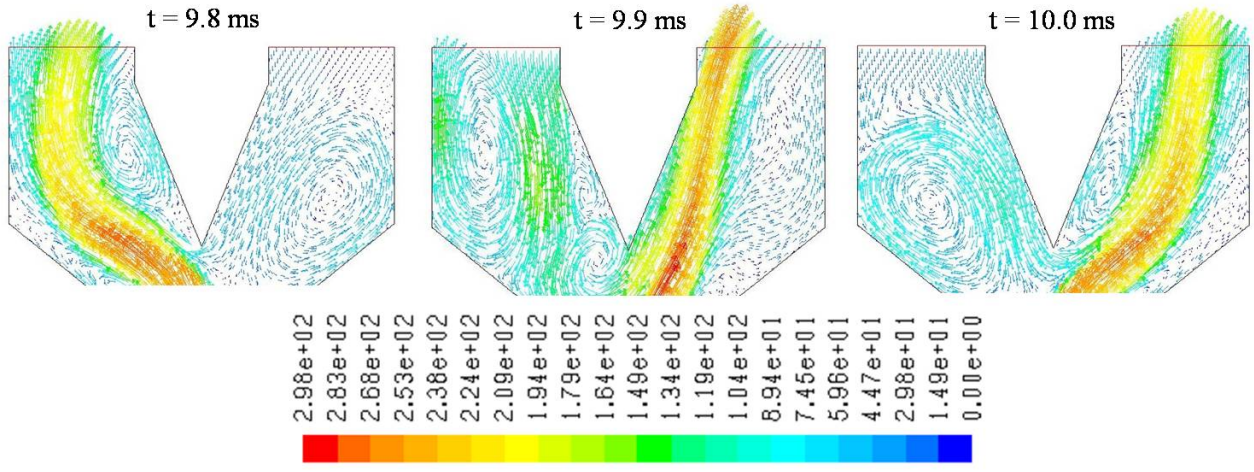

Figure 16.—Ma = 0.9, velocity vectors (m/s, scale shown sideways) snapshots taken at indicated times (ms) showing flow direction (suction) at exit planes, recirculation rolls, and stagnation zones in outlet channels.

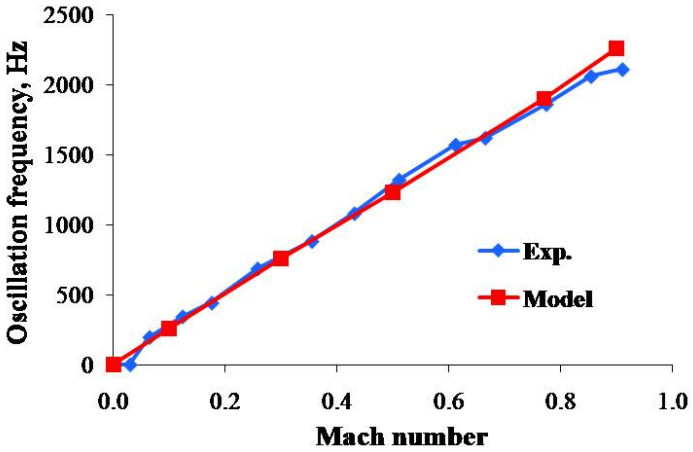

Figure 17.—Comparison of calculated and measured oscillation frequencies of the fluidic diverter versus Mach number.

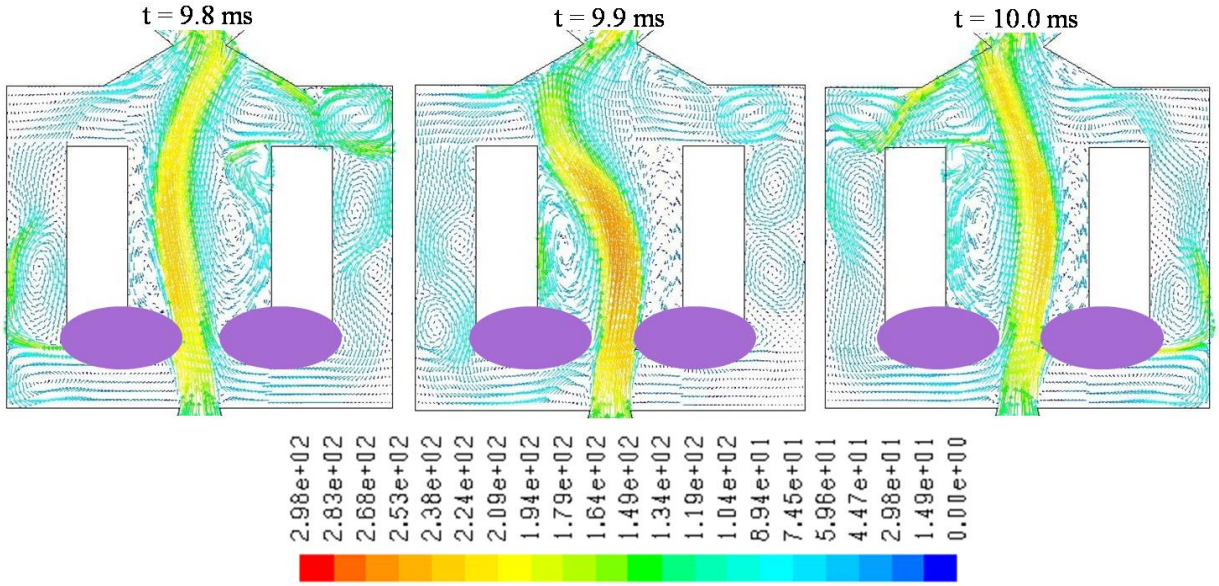

Figure 18.—Ma = 0.9, velocity vectors (m/s, scale shown sideways) snapshots taken at indicated times (ms) showing flow direction, recirculation rolls, and stagnation zones in central cavity and feedback channels.

It is also remarkable that, during oscillatory flow, the feedback channels on both sides of the central cavity are filled with either many recirculating "donut" rolls or the return flow towards the bottom nozzle exit, switching from one to the other depending on the stage of the oscillatory cycle (see Figs. 12 and 15). Figure 18 provides a clearer demonstration of this flow phenomenon by a series of velocity vector snapshots taken at 9.8, 9.9, and 10.0 ms spanning the same half-cycle duration as in Figure 16. The return flow in one of the feedback channels imparts momentum from one side onto the jet being issued from the bottom nozzle which causes the jet to bend towards the other side. The jet then enters the central wall-attachment section, is further influenced by the Coanda effect, and generates the diverted motion in the central cavity. This motion in the cavity leads to a return flow in the other feedback channel which eventually establishes the oscillatory behavior in the outlets.

It is curious to study the effects of acoustic speed and momentum exchange within the fluidic diverter as they relate to generating and sustaining the oscillations. It has been indicated that both fluid inertia and acoustic waves affect the speed of the feedback signal (Ref. 11). Since the dimensions of the specific

fluidic diverter studied in this paper, such as the length of the feedback channels, are fixed, the actual physical mechanism governing the creation and frequency of oscillations is explored by varying the acoustic speed in the fluid medium. Based on the kinetic theory prediction that the acoustic speed varies directly with the square root of temperature and inversely with the square root of the molecular weight of the gaseous medium, these two parameters have been varied in the numerical calculations. Replacing air by helium at 298 K and increasing the temperature of air from 298 to 1200 K have enabled us to increase the acoustic speed by more than a factor of two relative to our original baseline case. The results are shown in Figure 19 where the equivalent Mach number for air at 298 K is calculated by multiplying the actual Mach number of each case (obtained from plenum-to-exit pressure ratio) by the factors of square-root molecular-weight ratio or square-root temperature ratio. Note that the ratio of the specific heats at constant pressure and at constant volume for diatomic air ($\gamma = 1.40$) and for monatomic helium ($\gamma = 1.67$) is different, but for practical purposes, we neglected the effect of this ratio (basically a factor of $(1.67/1.40)^{1/2} = 1.09$) on the calculations. The actual individual Mach numbers for the helium case are 0.1 and 0.3 (green triangles), and for the 1200 K case are 0.1, 0.3, and 0.5 (pink circles), respectively. The preserved linearity of the calculated oscillation frequency when plotted against the equivalent Mach number is indicative of the fact that the physical mechanism scales with the acoustic speed in the gaseous medium. Note that the equivalent Mach number for air at 1200 K, for which the actual Mach number used in the numerical computation is 0.5, becomes slightly more than unity, but still seems to follow the linear trend.

The time for the first onset of instability leading to oscillations, called here the start delay time, is shorter for faster flows as mentioned above (see Figs. 11 and 14). The oscillation start delay time is plotted against the equivalent Mach number in Figure 20. The results for air at 298 K, shown by the black symbols and the connecting lines, represent our baseline case for which the equivalent Mach number is

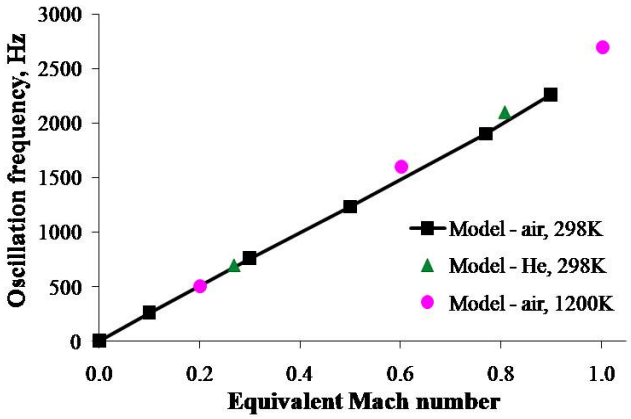

Figure 19.—Calculated oscillation frequency versus Mach number equivalent to that of air at 298 K.

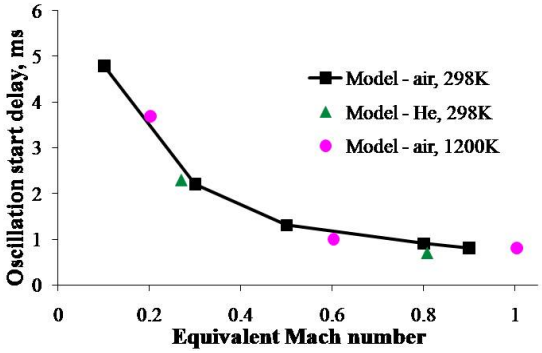

Figure 20.—Initial delay time (ms) for oscillations to start versus equivalent Mach number.

the same as the Mach number. It can be seen that the oscillation start delay time declines steadily as the flow rate increases and levels off as the Mach number approaches unity, suggesting that this phenomenon is also related to acoustic speed and reaches a minimum as the flow starts to choke. Indeed, when the acoustic speed in the gaseous medium is varied by replacing air with helium gas or by raising the air temperature to 1200 K, the oscillation start delay time follows the same trend with respect to the equivalent Mach number, i.e., the continuity of the original curve is not affected when the Mach number is scaled properly. Note again that, for the 1200 K case where the equivalent Mach number slightly exceeds unity, the oscillation start delay time levels off at a minimum, confirming a choking behavior. The behavior at higher (supersonic) Mach numbers will be studied elsewhere.

Conclusions

A time-dependent computational analysis of a specific fluidic diverter is conducted with an objective to develop an understanding of its self-induced internal flow oscillations. The goal is to utilize this information to improve its performance efficiency towards minimizing pressure losses for flow control applications. The velocity, temperature, and pressure fields are calculated up to sonic conditions. It is determined that the frequency of oscillations increases linearly with the flow rate (Mach number) through the fluidic diverter. The predicted oscillation frequencies have excellent agreement with our experimental measurements of the device. The delay time for the instability of the initially symmetric flow to develop and for the steady, periodic oscillations between the two outlets to start is shown to decrease with flow rate and levels off at a minimum as the Mach number approaches unity.

Dimensions of the specific fluidic diverter studied in this paper, such as the length of the feedback channels, are fixed, thereby limiting the parameter space of exploring the physical mechanisms of self-induced oscillations such as momentum and acoustic feedback. Yet, the observed evidence obtained by varying the flowing gas (air versus helium) and the operating temperature (298 versus 1200 K) for the range of Mach numbers used in this study indicates that the acoustic speed in the gaseous medium is a key factor in governing the mechanism of initiating the oscillations as well as determining its frequency.

The concept of using plasma actuation is employed in steady-state calculations to check the feasibility of producing oscillation frequencies of our own choosing instead of being dependent on the fixed-geometry fluidic device. It is determined that a very small plasma perturbation level, simulated by a numerical patch of T = 1300 K in a localized area, is sufficient to break the steady-state flow symmetry or switch the flow direction when the steady-state flow is already biased in one direction.

We plan to investigate the operation of the device at higher Mach numbers, as well as use the current numerical model for design optimization of the fluidic diverter and similar unsteady fluidic actuators.

References

1. Gad-el-Hak, M., *Flow Control: Passive, Active, and Reactive Flow Management*, Cambridge, New York Cambridge University Press, 2000. ISBN 0521770068 9780521770064.
2. Culley, D.E., Bright, M.M., Prahst, P.S., and Strazisar, A.J., "Active Flow Separation Control of a Stator Vane Using Embedded Injection in a Multistage Compressor Experiment," *Journal of Turbomachinery*, Vol. 126, No. 1, January, 2004, pp. 24–34.
3. Kirtley, K.L., Graziozi, P., Wood, P., Beacher, B., and Shin, H.-W., "Design and Test of an Ultra-Low Solidity Flow-Controlled Compressor Stator," GT2004–53012, Proceedings of the International Gas Turbine Institute, June 2004.
4. Guyot, D., Taticchi Mandolini Borgia, P., Paschereit, C.O., and Raghu, S., "Active Control of Combustion Instability Using a Fluidic Actuator," AIAA–2008–1058, 46th AIAA Aerospace Sciences Meeting and Exhibit, 7–10 January 2008, Reno, Nevada.
5. Coanda, H., "Device for Deflecting a Stream of Elastic Fluid Projected into an Elastic Fluid," United States Patent 2,052,869, Issued September 1, 1936.

6. Metral, A., “Sur un Phenomene de Deviation des Vienes Fluides et Ses Applications (Effect Coanda),” *Proceedings of the 5th International Congress for Applied Mechanics*, Cambridge, MA, 1939.
7. Feikema, D. and Culley, D. “Computational Fluid Dynamic Modeling of a Fluidic Actuator for Flow Control,” AIAA–2008–557, 46th AIAA Aerospace Sciences Meeting and Exhibit, 7–10 January 2008, Reno, Nevada.
8. Gregory, J.W., Ruotolo, J.C., Byerley, A.R., and McLaughlin, T.E., “Switching Behavior of a Plasma-Fluidic Actuator,” AIAA–2007–0785, Reno, NV, Jan. 2007.
9. Brown, C.A., “Scalability of the Localized Arc Filament Plasma Actuators,” AIAA–2008–3043, 14th AIAA/CEAS Aeroacoustics Conference, 5–7 May, 2008, Vancouver, British Columbia, Canada.
10. Kelecy, F.J., “Coupling Momentum and Continuity Increases CFD Robustness,” *ANSYS Advantage*, Vol. II, Issue 2, 2008, pp. 49–51.
11. Tesar, V., Hung, C.-H., and Zimmerman, W.B., “No-moving-part hybrid-synthetic jet actuator,” Sensors and Actuators A, Vol. 125, 2006, pp. 159–169.

REPORT DOCUMENTATION PAGE		Form Approved OMB No. 0704-0188

1. REPORT DATE *(DD-MM-YYYY)*	2. REPORT TYPE	3. DATES COVERED *(From - To)*
01-12-2009	Technical Memorandum	

4. TITLE AND SUBTITLE
Numerical Studies of a Fluidic Diverter for Flow Control

5a. CONTRACT NUMBER

5b. GRANT NUMBER

5c. PROGRAM ELEMENT NUMBER

6. AUTHOR(S)
Gokoglu, Suleyman, A.; Kuczmarski, Maria, A.; Culley, Dennis, E.; Raghu, Surya

5d. PROJECT NUMBER

5e. TASK NUMBER

5f. WORK UNIT NUMBER
WBS 561581.02.08.03.17.03

7. PERFORMING ORGANIZATION NAME(S) AND ADDRESS(ES)
National Aeronautics and Space Administration
John H. Glenn Research Center at Lewis Field
Cleveland, Ohio 44135-3191

8. PERFORMING ORGANIZATION REPORT NUMBER
E-17132

9. SPONSORING/MONITORING AGENCY NAME(S) AND ADDRESS(ES)
National Aeronautics and Space Administration
Washington, DC 20546-0001

10. SPONSORING/MONITOR'S ACRONYM(S)
NASA

11. SPONSORING/MONITORING REPORT NUMBER
NASA/TM-2009-216088; AIAA-2009-4012

12. DISTRIBUTION/AVAILABILITY STATEMENT
Unclassified-Unlimited
Subject Category: 01
Available electronically at http://gltrs.grc.nasa.gov
This publication is available from the NASA Center for AeroSpace Information, 443-757-5802

13. SUPPLEMENTARY NOTES

14. ABSTRACT
The internal flow structure in a specific fluidic diverter is studied over a range from low subsonic to sonic inlet conditions by a time-dependent numerical analysis. The understanding will aid in the development of fluidic diverters with minimum pressure losses and advanced designs of flow control actuators. The velocity, temperature and pressure fields are calculated for subsonic conditions and the self-induced oscillatory behavior of the flow is successfully predicted. The results of our numerical studies have excellent agreement with our experimental measurements of oscillation frequencies. The acoustic speed in the gaseous medium is determined to be a key factor for up to sonic conditions in governing the mechanism of initiating the oscillations as well as determining its frequency. The feasibility of employing plasma actuation with a minimal perturbation level is demonstrated in steady-state calculations to also produce oscillation frequencies of our own choosing instead of being dependent on the fixed-geometry fluidic device.

15. SUBJECT TERMS
Flow control; Fluidic actuators; Fluidic diverters; Numerical modeling

16. SECURITY CLASSIFICATION OF:			17. LIMITATION OF ABSTRACT	18. NUMBER OF PAGES	19a. NAME OF RESPONSIBLE PERSON
a. REPORT	b. ABSTRACT	c. THIS PAGE			STI Help Desk (email:help@sti.nasa.gov)
U	U	U	UU	24	19b. TELEPHONE NUMBER *(include area code)* 443-757-5802